Thermal Response of a Continuous Two-Span Composite Bridge Structure

Jack H. Emanuel, Department of Civil Engineering, University of Missouri-Rolla
David J. Wisch, Central Offshore Engineering, Texaco, New Orleans

This experimental investigation was conducted to verify and substantiate a prior theoretical study of environmental stresses induced in composite-girder bridge structures. The objectives of the study were (a) to construct and instrument a 4.6- and 4.6-m (15- and 15-ft) continuous two-span laboratory structure of composite design, (b) to subject the structure to thermal loading, and (c) to correlate the experimental temperature distributions, strain distributions, and deflections with those obtained from the theoretical study. Infrared heat lamps were used to obtain steady-state thermal loading. Three theoretical cases were considered for strain calculations: (a) both the slab and the beam in plane stress, (b) the slab in plane strain and the beam in plane stress, and (c) the slab in some state between plane stress and plane strain (partially restrained) and the beam in plane stress. The experimental and theoretical temperature distributions, strains, and deflections were in reasonable agreement. It was concluded that the theoretical procedure provides a rational method for predicting the thermal behavior of composite-girder bridge structures and can be applied with reasonable confidence when used with realistic temperature profiles, material properties, and substructure stiffness characteristics.

Bridge problems related to temperature have been the subject of rather extensive studies in Australia, Europe, Canada, and, to a lesser extent, the United States (1-11). However, the Australian and European studies have been concerned primarily with concrete box-girder structures rather than with concrete-steel composite-design bridges. The temperature-distribution analysis involved in these two types of design differs very little, but the determination of strains and stresses differs markedly.

A single-material structure has deformations and stresses that result from nonlinear thermal gradients and from restraints acting at the abutments. Structures made of two or more dissimilar materials have, in addition to the above factors, internal stresses and strains caused by the interaction of differing physical properties and require a complex analysis. Recent numerical studies have shown that thermally induced stresses in a composite-design structure can reach 30-40 percent of the design strength of the component materials (6, 8, 10).

Designers of many recent bridges have eliminated expansion devices in favor of connecting the superstructure to a flexible substructure (12, 13). Recent rigorous studies (8, 10, 14) investigated thermally induced stresses in this type of structure from a theoretical standpoint. Acceptance of the developed procedures and theoretical results and their use in design criteria are subject to substantiation by experimental results obtained from model and prototype testing.

The objectives of this study were to design, construct, and instrument a small composite-design laboratory structure; to subject the structure to thermal loading; and to correlate the experimental results with calculated values obtained by using the theoretical procedures previously developed (10, 14). Both the temperature distribution and the thermally induced strains and stresses were investigated.

TEST STRUCTURE

The test structure used was a 4.6- and 4.6-m (15- and 15-ft) two-span continuous composite-design bridge 114 cm (45 in) wide with no skew. A curved steel plate and pintle bearing was used at the pier, and integral abutments were used at the ends. For reasons of economy and mechanics, an adequate rather than a true model was designed and constructed.

Abutments

Integral stub abutments with flexible pilings were modeled by the test structure. Modeling considerations included a desire for a constant soil modulus, noninterference of the container on the soil medium and pile interaction, and a reasonable piling-to-superstructure stiffness ratio. The minimum dimensions of the medium container were based on ratios to avoid container interference suggested by Davisson and Salley (15) from model pile tests.

A uniform sand was chosen as the soil medium because it allowed the greatest control over the required soil parameters, which included low moisture content, ability to retain a constant modulus under repeated loading, a constant density, and the ability not to pick up moisture from the atmosphere. A uniform density of 1674 kg/m^3 (104.5 lb/ft^3) was achieved by using the "rain" placement method of Vesic (16). All sand was dried to less than 2 percent moisture by weight before placement to avoid modulus change and cementing.

Pilings, three at each end of the structure beneath the stringers, were steel bars 183 cm (72 in) long with a 127x13-mm (5x0.5-in) cross section buried 168 cm (66 in) in the sand. For ease of placement and to provide a rigid connection to the superstructure, a 152x13-mm (6x0.5-in) steel-plate pile cap was welded across the tops of the piles.

Pier, Bearings, Stringers, and Slab

Three standard pipe sections 5 cm (2 in) in diameter by 194 cm (76.5 in) long were rigidly attached to the floor and provided the pier. This simulated a cantilever beam, in accordance with the fact that in the field most piers have a relative point of fixity.

Stringer plates welded to the bottom flange of each stringer were bolted to the piling cap plate to create an integral connection at the abutments. This connection transferred both moment and rotation along with longitudinal displacement. The pier bearing consisted of curved steel plates attached to the stringers nesting on a machined bearing plate supported by the pier. Chamfered pintles were used to prevent displacement but allow rotation.

A miscellaneous-shape wide-flange section 15 cm by 64 N/m (M6 by 4.4) was selected for the three stringers spaced 51 cm (20 in) on center. Ten sets of channels

10 cm (4 in) deep were used for the diaphragms located at 0.6, 1.2, 2.6, 4, and 4.6 m (2, 4, 8.5, 13, and 15 ft) from each side of the pier. Stud shear connectors 10 mm (0.38 in) in diameter by 22 mm (0.88 in) were welded to the top flanges of the stringers at 10-cm (4-in) centers. In accordance with standard AASHTO procedures, connectors were not placed in high-tensile (negative-moment) zones. The steel layout is shown in Figure 1.

A 38-mm (1.5-in) slab depth was chosen to keep an acceptable slab-to-stringer stiffness ratio. A 16-gauge wire mesh was placed close to the top and bottom of the slab for reinforcement. The mesh provided reinforcement and temperature steel in the longitudinal and transverse directions. Crushed limestone with a maximum particle size of 10 mm (0.38 in) was used for the coarse aggregate; a masonry-blend sand was used for the fine aggregate; and the air content of the concrete was 6.3 percent. The 28-day strength obtained from cylinder tests was 30.3 MPa (4400 lbf/in^2).

INSTRUMENTATION

The task of the instrumentation was to record temperatures, strains, and displacements at selected points. The automatic data-recording system included an automatic scanner, a stepping unit, and a paper-tape perforator.

Carbon-steel temperature-compensated SR-4 strain gauges recorded apparent strain. Gauges on the center stringer and in the slab were mounted with a heat-cure epoxy to minimize creep and adhesive deterioration. Thermistors that had a sensitivity of ±0.2°C (0.4°F) were mounted near each strain group with a metal-filled epoxy for better heat transmission. Gauges and thermistors were mounted directly on steel surfaces at all locations except those in the concrete deck.

To obtain reliable readings in the slab, the instrumentation was mounted on high-grade soda-lime glass microscope slides of low alkali content. The mechanical and thermal properties of the glass slides, which were 2.5 mm (0.10 in) thick, were very close to the properties of the concrete deck. This reduced the possibility that heat sinks would alter temperature gradients and that dissimilar coefficients of thermal expansion and Young's moduli would induce stress concentrations. To provide a better mechanical bond to the deck concrete, several 6.4x3.2-mm (0.25x0.13-in) slots were cut into the sides of the slides.

Instrumentation exposed to the atmosphere was moistureproofed with a neoprene barrier, while that in the deck was coated with several thin layers of beeswax. All leads from the gauges to the system were of the same length.

The total longitudinal deck deflection and vertical deflection at the midspans were recorded by using dial indicators with a least count of 0.025 mm (0.001 in). Indicators at the midspans were mounted on wooden standards, whereas those at the abutments were attached to metal channels that were rigidly attached to the sand-box frame.

All information except the indicator readings could be recorded through the acquisition system and output on paper tape. This tape was then read into a minicomputer that formatted and sent the recorded values through a remote terminal directly into data files of an IBM 360-70 for data reduction.

Instrumentation Orientation

Pairs of strain gauges were mounted on the center pier 10 cm (4 in) and 46 cm (18 in) above the floor. The gauges were mounted on opposite faces to record pier bending if the top translated toward either abutment.

Five locations along the length of the bridge were chosen for the placement of transducer groups. Two groups were placed midway between stringers near the abutments and had transducers in the deck only. The other three locations were along the center stringer and had transducers through the slab and on the stringer. The location of each group is shown in Figure 2.

Transducers placed in the slab consisted of a microscope slide with a strain gauge, thermistor, and leads as shown in Figure 3. These transducers were located at the top and four intermediate points of the slab, and thermistors and strain gauges were placed on the stringer flanges and at seven intermediate points on the web at locations 2, 3, and 4, as shown in Figure 4.

Locations 1 and 5 had instrumentation in the slab only. The transducers were placed in cantilever temperature-reference bars measuring 23 cm (9 in) longitudinally by 10 cm (4 in) transversely and separated from the deck on three sides by flexible Styrofoam and void of wire mesh. The Styrofoam provided virtually no resistance to small expansive movements and allowed thermal gradients, which would have been altered had there been an air space instead of the insulating material, to remain continuous along the deck.

Thermistors were also positioned 7.6, 15, and 30 cm (3, 6, and 12 in) above and below the slab to give an indication of the still air temperature and the thermal gradients around the bridge. The thermistors above the deck were shaded from the heat lamps to avoid the effect of incident radiation on unshielded thermistors.

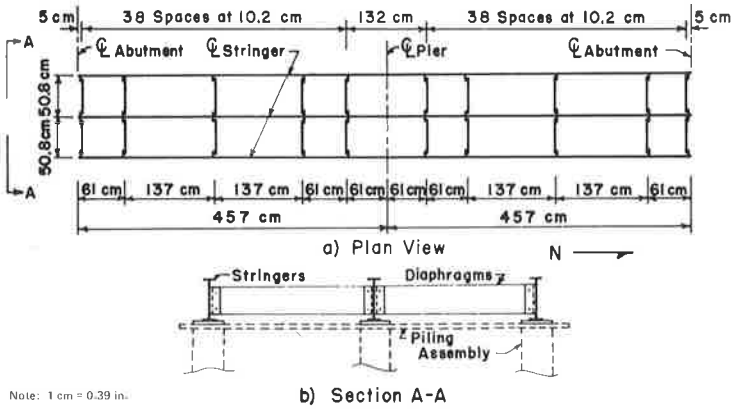

Figure 1. Steel layout.

TESTING

Heat Source

The test structure was thermally loaded by using 250-W infrared reflector heat lamps. Radiation heating rather than a constant heat source (i.e., heated fluid) was chosen because it more closely approximated actual field conditions and was simple to control. The lamps were placed in four rows along the length of the bridge, and alternate rows were staggered to provide a more uniform distribution. The faces of the lamps were placed 51 cm (20 in) above the deck. This height provided a deck temperature up to 72°C (160°F) and uniform radiation distribution.

The 120 lamps were divided into five circuits. Three circuits controlled the perimeter lamps, and each of the other two circuits controlled an interior row of lamps. To obtain uniform radiation incident across the width of the deck, the outer lamps required a higher voltage, because there was less overlapping along the edges than in the center. Each circuit was controlled by a Variac transformer. Thus, different levels of uniform thermal loading could be obtained.

To check the uniformity of the thermal loading, a heat receptor was fabricated and painted flat black. When the receptor indicated a constant temperature at all locations on the deck, the circuits were considered to be adjusted properly for the most uniform heat flux.

Figure 2. Plan view of deck instrumentation groups.

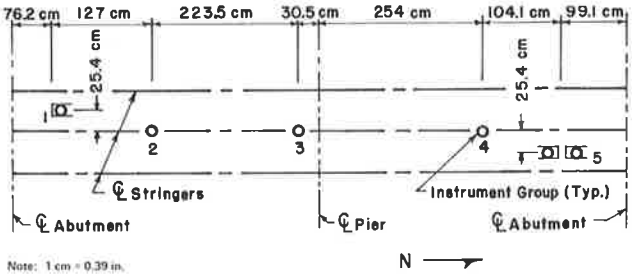

Figure 3. Slab transducer.

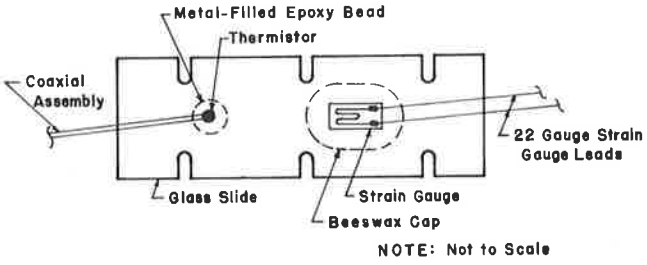

Figure 4. Slab and stringer instrumentation.

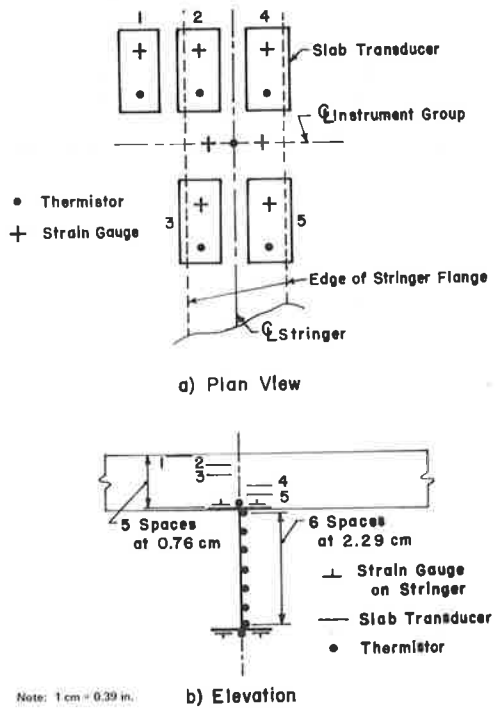

Testing Procedure

Before any testing cycle, the laboratory was sealed to eliminate any outside drafts or drafts from heat and air-conditioning ducts. Thus, the only source of forced convection would be air currents caused by thermal gradients developing into cyclic drafts as a result of the laboratory's size.

Steady-state temperatures through the cross section were achieved after seven hours of heating. Strain-gauge and thermistor readings were recorded on punched tape through the acquisition system. Dial-indicator readings were hand recorded. Recorded values included longitudinal strains and temperatures at previously described points, strains at the base of the pier to determine the lateral movement of the top of the pier, and the ambient air temperatures at points above and below the slab.

THERMAL STRESSES

Analysis of thermal strains and stresses in an indeterminate structure is achieved by (a) removing redundants to obtain a determinate structure, (b) dividing the simple determinate structure into a number of constant-section segments and determining the thermally induced segment strains and stresses, (c) applying the redundants as loads and obtaining by conventional methods of analysis the resultant induced stresses and strains caused by the redundants, and (d) superimposing the thermally induced and the redundantly induced strains and stresses.

A procedure for determining thermally induced strains and stresses was developed by Zuk (1, 2) and modified by Berwanger (17) and Berwanger and Symko (6). Emanuel and Hulsey (8) and Hulsey (10) refined the work of Zuk and of Berwanger and developed a procedure to account for slab-beam interaction.

The procedure used in this study follows that of Hulsey (10). The geometric and material segment properties are assumed to be constant along the segment length; the temperature profile through the depth of the cross section is assumed to be constant along the segment length; and the slab and stringer are assumed to form a composite section. The slab may be assumed to be in plane stress ($\sigma_z = 0$), plane strain ($\epsilon_z = 0$), or some state between the two. The beam is assumed to be in a state of plane stress for all cases. Theoretical results for each of the three cases were compared with experimental results in this investigation.

TEMPERATURE DISTRIBUTION

The temperature distribution through a bridge structure

has been a popular research topic in recent years for both steady-state and transient conditions. Due to complexity of the (a)governing differential equations arising from the geometry of the structure, (b) boundary conditions, and (c) effects of all three classical forms of heat transfer, solutions for the distribution have centered on numerical techniques.

The numerical technique chosen for theoretical solutions in this study was a finite-element technique originally developed by Wilson and Nickell (18) and extended by Hulsey (10). This technique was a two-dimensional analysis capable of handling multiple materials, nonlinear boundary conditions, all three classical forms of heat transfer, and steady and transient conditions.

RESULTS OF EXPERIMENTAL INVESTIGATION

In the test sequence, two levels of radiation were applied to the deck, and multiple tests were made at each level. At the higher level a heat flux of 0.06 W/cm^2 (1.30 Btu/in^2·h) was incident on the surface, while at the lower level 0.05 W/cm^2 (1.13 Btu/in^2·h) was incident.

Temperature Distribution

Very consistent repeated-test results were obtained; temperature profiles for a given flux input fell within a 3°C (5.4°F) band. Profiles taken along the length of the bridge, at locations 2, 3, and 4, also fit within this band. Experimental profiles for a typical test at the maximum flux level are shown in Figure 5. Temperature profiles for reduced-power tests, being 8.7°C (15.6°F) cooler at the top of the slab and 4°C (7.2°F) cooler at the bottom of the stringer, parallel those of Figure 5.

Figure 5. Experimental and theoretical temperature profiles for typical full-power test.

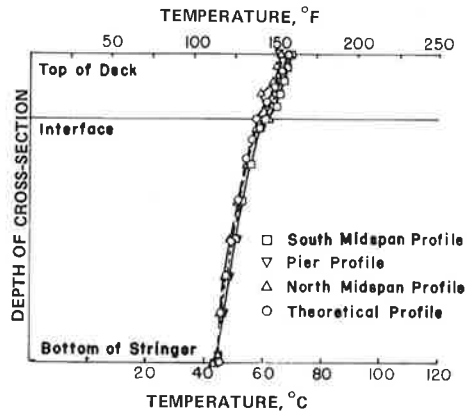

The theoretical temperature profiles were obtained from a finite-element analysis. The variables used in the analysis are tabulated below [1 W/cm^2 = 22.03 Btu/in^2·h; 1 W/cm·°C = 57.78 Btu/ft·h·°F; 1 W/m^2·°C = 0.18 Btu/ft^2·h·°F; t°C = (t°F - 32)/1.8].

Property	Trial 1	Trial 2
Heat flux (W/cm^2)	0.059	0.051
Deck absorptivity	0.7	0.7
$k_{concrete}$ (W/cm·°C)	0.014	0.014
k_{steel} (W/cm·°C)	0.538	0.538
$h_{above\ deck}$ (W/m^2·°C)	6.92	6.92
$h_{below\ deck}$ (W/m^2·°C)	4.14	4.14
$Air_{above\ deck}$ (°C)	49	104
$Air_{below\ deck}$ (°C)	35	32

The convective-film-coefficient ratio that was selected varied slightly from those suggested by Emerson (3) and Priestly (9) for a horizontal plane surface to account for the vertical projection of the stringer webs. Air temperatures were based on laboratory readings taken during testing.

The excellent correlation between the theoretical and the experimental profiles is shown in Figure 5.

Strain Distribution

The recorded strains included apparent strain resulting from the effects of change in electrical resistance (a result of higher-than-average test temperatures), restraints (abutments and pier), and dissimilar materials. An apparent strain resulting from a difference in thermal coefficients of expansion was also induced in the glass-slide transducers. A computer program was developed for data reduction and apparent-strain correction.

The repeated-test bandwidth for as-recorded and temperature-compensated strain profiles is shown in Figure 6. Strains for repeated tests fall within a narrow bandwidth similar to that observed for the temperature profiles.

Figure 6. Strain profiles, south midspan, full-power tests.

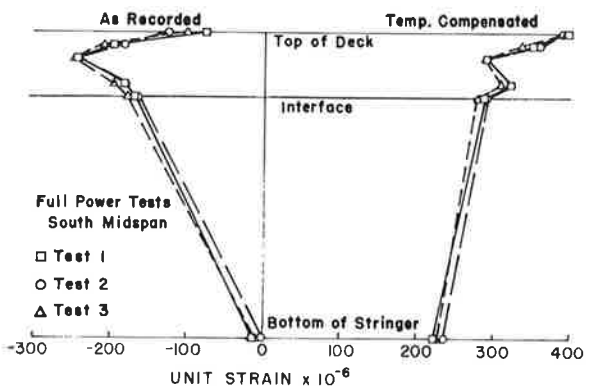

The relation among the experimental strains along the length of the bridge, i.e., at instrument groups 2, 3, and 4, is shown in the as-recorded and compensated strain test profiles of Figure 7.

In contrast to the temperature profiles, an erratic pattern of strains is apparent in the slab. These patterns could be the result of a number of things such as imperfect bonding or slippage between the transducers and the deck or honeycombs or air voids in the concrete around the instrument groups. The latter could result from inadequate emplacement of the concrete around the congestions of transducers in the slab. All patterns, however, are consistent for a given series of tests.

From the data obtained from the cantilever reference sections of instrument groups 1 and 5, the coefficient of thermal expansion for the limestone-aggregate concrete was determined to be (6.3×10^{-6})/°C [(3.5×10^{-6})/°F]. This compares closely with calculated design values obtained from the method of Emanuel and Hulsey (19). The experimental value is used later in calculations of theoretical strains.

The strain profiles indicate negative curvature (lengthening of top deck fibers greater than that of bottom flange fibers) at the midspan locations and positive curvature above the center pier. These relation-

Figure 7. Experimental and theoretical strain profiles for test 2, full-power flux level.

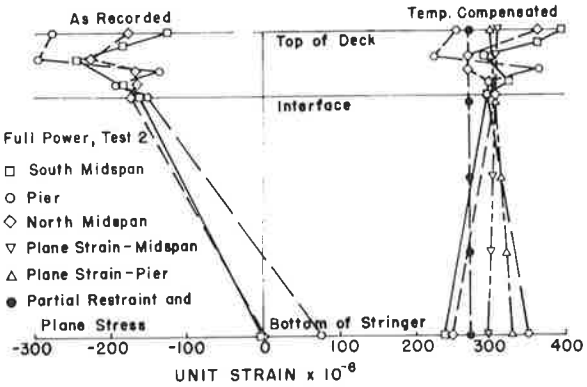

Figure 8. Distorted line diagram of relative thermally induced superstructure deformations.

ships are compatible with the temperature profiles (i.e., the top of the section is warmer than the bottom) and with the pier support, which arrests dead-load deflection at the support.

There was no differential strain at the base of the pier, which indicates that no longitudinal displacement occurred at the bearing elevation of the pier and thus that longitudinal displacements were symmetrical about the center of the structure. This symmetrical action was substantiated by the dial-indicator readings (slightly less than 0.13 mm [0.05 in]) at each of the abutments that were virtually identical for each of the tests in a given series.

Strains recorded from the piling gauges were very erratic, and no plausible explanation, conclusions, or trends could be deduced.

The previously described procedure of Emanuel and Hulsey (8) and the computer program developed by Hulsey (10) were used to obtain the theoretical strains. Experimental rather than the theoretical temperature profiles were used to calculate the theoretical strains that were correlated with the experimental strains. The following material properties were used to calculate the theoretical values [1 Pa = 0.000 145 lbf/in^2; t°C = (t°F - 32)/1.8].

	Value	
Property	Steel	Concrete
Young's modulus (Pa)	2.1×10^{11}	2.1×10^{10}
Poisson's ratio	0.3	0.2
Coefficient of thermal expansion	11.7×10^{-6}/°C	6.3×10^{-6}/°C

The three cases analyzed were (a) both the slab and the beam in plane stress, (b) the slab in plane strain and the beam in plane stress, and (c) the slab in some state between plane stress and plane strain (partially restrained) and the beam in plane stress. The theoretical strain profiles for the three cases are shown for the full-power flux level in Figure 7. The profiles for reduced power parallel those in Figure 7 (20 $\mu\epsilon$ lower).

The uncommon coincidence of the midspan and the pier profiles for case a, slab in plane stress, and case c, slab partially restrained, results from the particular combination of material and cross-sectional geometric properties and the temperature profiles of the test structure. The vertical orientation of the profiles indicates very little longitudinal curvature of the cross section at midspan and pier, which results in very small calculated vertical deflections at the midspan.

The experimental and the theoretical strains show close general agreement. Also, the observed and theoretical longitudinal deck displacements at the bearing elevation of the abutments differ by only 10-15 percent of the measured and theoretical values.

The only experimental and theoretical values not in reasonable agreement, excluding strain scatter in the slab, are the vertical deflections at the midspans and the curvatures at both the midspan and the pier. These deflections and curvatures are both functions of differential strain values and the vertical distance between the points of strain measurement. The closest agreement between experimental and theoretical curvature is for case b, the slab in plane strain. This case also yielded the largest theoretical calculated vertical deflection, about 25 percent of the observed deflection and a rather poor correlation. However, the experimental strains yield a curvature that would produce deflections quite close to those observed.

The most plausible explanation for differences in correlation originates at the pier. The programmed theoretical procedure assumes (a) a continuous shear connector spacing, which results in an assumed stiffer structure, and (b) that no vertical displacement occurs at any support. In the test structure, some vertical deflection was possible at the pier. As a result of the curved steel rocker plate and pintle, the superstructure was free to deflect vertically upward at the pier, the only restrictions being its own dead weight and the stiffness of the structure (as with a prototype structure). The effect of this vertical deflection would be to increase the curvature above the theoretical values and subsequently to increase the midspan deflections. Vertical deflections (upward) measured at the pier during the tests were approximately 0.25 mm (0.01 in), which was slightly less than one-third the deflection of about 0.76 mm (0.03 in) at the midspan. The vertical deflection at the abutments was negligible. A distorted line diagram of relative thermally induced superstructure deformations is shown in Figure 8.

Determination of stress in the theoretical procedure uses the interaction of longitudinal, transverse, and vertical strains and Poisson's ratio, longitudinal strains being the major parameter. In this study, it was feasible to instrument only for longitudinal strain. Thus, a prediction of stress based strictly on experimental observation is not possible. However, because the experimental and theoretical longitudinal strains correlate closely, theoretical stresses calculated from the observed temperature profile are believed to be valid and are presented below (1 kPa = 0.145 lbf/in^2) for full-power tests and discussed in what follows. The pattern of stresses for reduced-power tests parallels those for full-power tests.

	Stress		
Location	Case a	Case b	Case c
Top of slab			
Midspan (kPa)	62	-214	-324
Pier (kPa)	76	-290	-303

Location	Stress		
	Case a	Case b	Case c
Bottom of slab			
Midspan (kPa)	965	820	1820
Pier (kPa)	965	786	1820
Top of stringer			
Midspan (MPa)	-30.2	-22.7	-33.7
Pier (MPa)	-30.2	-23.0	-33.6
Bottom of stringer			
Midspan (MPa)	8.2	13.2	8.6
Pier (MPa)	7.9	20.3	7.9

Case c, the slab in some state between plane stress and plane strain, produces the highest compressive thermal stress in the upper flange of the stringer at both the midspan and the pier. Values for case a are not quite 10 percent lower and for case b are 40 percent lower.

Tensile stresses are produced in the lower stringer flange. The highest values at both midspan and pier are found with method b and slightly lower values result from methods a and c in order of magnitude, respectively.

For flange stresses, the method producing the largest compressive stresses produced the smallest tensile stresses, and vice versa.

The maximum compressive stress [33.7 MPa (4890 lbf/in^2)] in the upper flange occurred at midspan for case c and was approximately 25 percent of the allowable design stress. The maximum tensile stress [20.3 MPa (2440 lbf/in^2)] in the bottom flange occurred at the pier for case b and was nearly 15 percent of the design stress.

Maximum tensile and compressive slab stresses at both the midspan and the pier were produced by case c. This is caused primarily by transverse bending in the slab between the stringers. The maximum slab tensile stress [1820 kPa (264 lbf/in^2)] and the maximum compressive stress [303 kPa (44 lbf/in^2)] were approximately 10 and 3 percent of the compressive strength of commonly used 20.7-MPa (3000-lbf/in^2) concrete.

The theoretical procedure is based on the assumption that the pier does not deflect vertically. Upward pier-support movement, indicated in the tests, reduces the tensile stress in the lower stringer flange; however, this movement has only minimal effect on the stress in the upper flange, because this flange is very near the neutral axis of the composite section.

Integral abutments, as contrasted with roller supports, introduce the following effects. As the substructure stiffness increases, changes in the longitudinal stress patterns result primarily from the interaction of axial (P/A) and flexural (My/I) stresses produced by the resistance to movement at the abutments. At midspan, the primary influence is an My/I superposition from a moment that induces positive curvature. This results from the resistance of the stiffer abutment (piling) to rotation of the superstructure. This rotational resistance also reduces the curvature and deflections along the span adjacent to the abutment.

If there is no vertical deflection at the pier, the My/I effect at the pier is produced by a moment that induces negative curvature. This results from decreasing deflection at midspan. The reduced negative curvature at midspan helps produce reduced positive curvature at the pier.

The P/A effect is present at both pier and midspan but has less effect on the stresses at any given cross section than does an increase in abutment rotational stiffness. However, if an approach slab abuts the superstructure or abutment cap and resists longitudinal movement, the P/A effect can become very significant.

It should be noted that the theoretical trends discussed are based on the assumption that the center pier does not deflect vertically. If vertical movement occurs, the theoretical values should be modified by the resultant My/I effect for more accurate results.

CONCLUSIONS

Based on the correlation of consistent readings from multiple runs at two levels of steady-state infrared radiation heat loading and calculated theoretical values, the conclusions that follow were reached.

1. Steady-state temperature profiles can be predicted with reasonable accuracy from the modeling procedures used for the study. These procedures provide an upper bound for both temperatures and subsequent calculated stresses. Actual temperature profiles are generally lower than the modeled steady-state profiles because of the variation in and short duration of given values of the incident heat flux that strikes the surface, whereas the steady-state analysis requires several hours of constant flux application. Wind also tends to reduce temperatures.
2. The correlation confirms that the theoretical procedures are adequate for a reasonable prediction of the behavior of composite-girder bridge structures subjected to thermal loading.
3. The theoretical longitudinal curvature is somewhat smaller than that observed. This is believed to be a result of the assumption that there is no vertical deflection of the supports, whereas the test data indicate an upward deflection of the pier.
4. The theoretical and the observed longitudinal strains are in reasonable agreement. Resultant stresses in the test structure, which are functions of longitudinal, transverse, and vertical strains, can be expected to parallel the theoretical values.
5. Based on the strain profiles, the theoretical procedures give reasonable stress values for the slab and upper flange areas of the cross section. The theoretical stresses in the lower flange tend to be larger than they actually are. This is believed to arise from the My/I effect resulting from vertical deflection at the pier and is more pronounced in the lower flange because it is farthest from the neutral axis of the section.
6. A comparison of the experimental temperature profiles of the slab directly above the stringer and midway between the stringers indicates that case c is the most realistic of the three theoretical cases. The profile midway between stringers is more vertical (less temperature differential) than the profile directly above the stringer. This indicates transverse bending in the slab.
7. All three cases of the theoretical procedure will generally predict upper-bound stresses for a composite-girder bridge structure subjected to a steady-state radiant heat flux that has a coefficient of thermal expansion for the concrete lower than that of the steel.

Subject to the limitations of correlation with a single experimental test structure, it is concluded that the theoretical procedure provides a rational method for predicting the thermal behavior of composite-girder bridge structures and can be applied with reasonable confidence when used with realistic temperature profiles, material properties, and substructure stiffness characteristics.

Further substantiation and modification from field

testing of prototype structures to develop rational design criteria for thermal behavior are desirable and feasible.

RECOMMENDATIONS FOR FURTHER STUDY

During the course of any investigation, additional questions arise from the research. It is customary for most of these questions to be beyond the scope of the study and remain unanswered.

From a practical standpoint, the following topics could be of immediate value to the development of a simplified design procedure that would account for the thermal behavior of bridge structures and need to be conducted:

1. A study of the thermal behavior of the concrete deck in the transverse and vertical directions;
2. A study of the effect of diaphragms and supports on transverse action;
3. A determination of the effect of noncomposite areas on deck-stringer thermal interface forces and stress variations;
4. A study of the effect of slab reinforcing on the transfer of heat through a concrete bridge deck, i.e., temperature distribution;
5. A parametric study of the interaction of substructure stiffness, cross-sectional geometric properties, span lengths, material properties, and support deflections to establish limiting lengths for composite design structures on flexible substructures; and
6. Wind-tunnel studies on the effect of turbulent air flow on the convective film coefficient.

ACKNOWLEDGMENT

This research project, conducted as a Missouri Cooperative Highway Research Program study, was sponsored by the Missouri State Highway Department in cooperation with the Federal Highway Administration, U.S. Department of Transportation.

The opinions, findings, and conclusions expressed here are not necessarily those of the Federal Highway Administration. This report does not constitute a standard, specification, or regulation.

REFERENCES

1. W. Zuk. Thermal and Shrinkage Stresses in Composite Beams. Journal of the American Concrete Institute, Vol. 58, No. 3, Sept. 1961, pp. 327-340.
2. W. Zuk. Thermal Behavior of Composite Bridges—Insulated and Uninsulated. HRB, Highway Research Record 76, 1965, pp. 231-253.
3. M. Emerson. The Calculation of the Distribution of Temperature in Bridges. U.K. Transport and Road Research Laboratory, Crowthorne, Berkshire, England, Rept. LR 561, 1973.
4. A. G. Lanigan. The Temperature Response of Concrete Box Girder Bridges. School of Engineering, Univ. of Auckland, New Zealand, Ph.D. thesis, Rept. 94, 1973.
5. J. C. Reynolds and J. H. Emanuel. Thermal Stresses and Movements in Bridges. Journal of Structural Division, Proc., ASCE, Vol. 100, No. ST1, Paper 10275, Jan. 1974, pp. 63-78.
6. C. Berwanger and Y. Symko. Thermal Stresses in Steel-Concrete Composite Bridges. Canadian Journal of Civil Engineering, Vol. 2, No. 1, 1975, pp. 66-84.
7. B. Hunt and N. Cooke. Thermal Calculations for Bridge Design. Journal of Structural Division, Proc., ASCE, Vol. 101, No. ST 9, Paper 11545, Sept. 1975, pp. 1763-1781.
8. J. H. Emanuel and J. L. Hulsey. Thermal Stresses and Deformations in Nonprismatic Indeterminate Composite Bridges. TRB, Transportation Research Record 607, 1976, pp. 4-6.
9. M. J. N. Priestly. Linear Heat-Flow Analysis of Concrete Bridge Decks. Department of Civil Engineering, Univ. of Canterbury, Christchurch, New Zealand, Research Rept. 76-3, Feb. 1976.
10. J. L. Hulsey. Environmental Effects on Composite-Girder Bridge Structures. Univ. of Missouri-Rolla, Ph.D. thesis, 1976.
11. J. H. Emanuel and J. L. Hulsey. Temperature Distribution in Composite Bridges. Journal of Structural Division, Proc., ASCE, Vol. 104, No. ST1, Paper 13474, Jan. 1978, pp. 65-78.
12. C. E. Ekberg, Jr., and J. H. Emanuel. Current Design Practice for Bridge Bearings and Expansion Devices. Engineering Research Institute, Iowa State Univ., Ames, Final Rept., Project 547-S, 1967.
13. J. H. Emanuel and others. An Investigation of Design Criteria for Stresses Induced by Semi-Integral End Bents: Phase I—Feasibility Study. Missouri Cooperative Highway Research Program, Univ. of Missouri-Rolla, Final Rept. 72-9, 1973.
14. J. L. Hulsey and J. H. Emanuel. Finite Element Modelling of Climatically Induced Heat Flow. In Numerical Methods for Differential Equations and Simulation (A. W. Bennett and R. Vichnevetsky, eds.), North-Holland, Amsterdam, 1978, pp. 111-114.
15. M. T. Davisson and J. R. Salley. Model Study of Laterally Loaded Piles. Journal of Soil Mechanics and Foundations Division, Proc., ASCE, Vol. 96, No. SM5, Sept. 1970, pp. 1605-1627.
16. A. S. Vesic. A Study of Bearing Capacity of Deep Foundations. Engineering Experiment Station, Georgia Institute of Technology, Final Rept., Project B-189, 1967.
17. C. Berwanger. Thermal Stresses in Composite Bridges. Proc., ASCE, Specialty Conference on Steel Structures, Univ. of Missouri, Columbia, Engineering Extension Series 15, June 1970, pp. 27-35.
18. E. L. Wilson and R. E. Nickell. Application of the Finite Element Method to Heat Conduction Analysis. Nuclear Engineering and Design, No. 4, 1966, pp. 276-286.
19. J. H. Emanuel and J. L. Hulsey. Prediction of the Thermal Coefficient of Expansion of Concrete. Journal of the American Concrete Institute, Vol. 74, No. 4, April 1977, pp. 149-155.

Publication of this paper sponsored by Committee on General Structures.